J Electr Eng Technol Vol. 9, No. 4: 1385-1393, 2014
http://dx.doi.org/10.5370/JEET.2014.9.4.1385

ISSN(Print) 1975-0102
ISSN(Online) 2093-7423

On-line Temperature Monitoring of the GIS Contacts Based on Infrared Sensing Technology

Qingmin Li†, Haoxi Cong*, Jinyuan Xing, Bo Qi** and Chengrong Li****

Abstract – Gas insulated switchgear (GIS) is widely used in the power systems, however, the contacts overheating of the inside circuit breaker or disconnector may be a potential cause of developing accidents. As the temperature of the contacts cannot be directly acquired due to existence of the metallic shield, an infrared sensor is adopted to directly measure the temperature of the shield and then the contacts temperature can be indirectly obtained by data fitting, based on which the on-line temperature monitoring technology specifically for GIS contacts based on infrared sensing is proposed in this paper. A real GIS test platform is constructed and experimental studies are carried out to account for the influential factors that affect the accuracy of the infrared temperature measurement. A heat transfer model of the GIS module is also developed, together with experimental studies, the nonlinear temperature relationship among the contacts, the metallic shield and the environment based on a neural network algorithm is established. Finally, an integrated on-line temperature monitoring system for the GIS contacts is developed for on-site applications.

Keywords: GIS, Infrared sensing, Contact temperature, On-line monitoring, Neural network algorithm

1. Introduction

With vigorous development of the electric power industry and the growing demand of electricity, gas insulated switchgear (GIS) has been widely used in the power systems [1-2] and presents unique advantages including outstanding breaking capacity, long maintenance cycle, low failure rate, low maintenance costs, small occupation space, etc. However, if the contacts of the circuit breaker or the disconnecting switch within the GIS equipment are in poor status that gives an increased resistance, overheating phenomenon may occur when the load current flows through [3-4]. Overheating of the contacts and the lead conductor will result in reduced allowable load flow, and may cause insulation degradation or even breakdown accident [5-7]. According to previous available statistics, there have been varying degrees of abnormal temperature variation in the enclosed isolation switch and cable joints of the GIS equipment which is caused by poor contacts [8]. Hence, the on-line temperature monitoring of the GIS contacts used to identify and eliminate the developing thermal deficiency prior plays an irreplaceable significant role in safe and reliable operation of the GIS equipment.

Currently, there are three prevailing measures to monitor the GIS contacts overheating in field applications, including observation of the contact surface color [9], measurement of the loop resistance on a regular basis, and the temperature monitoring of some fixed points with infrared imager regularly [10-11]. However, the above methods are still flawed, for example, maintenance outage is sometimes indispensable, and the infrared imaging technology lacks of satisfactory resolution and accuracy to meet the requirements. Moreover, most of the prevailing methods encounter difficulty in achieving continuous temperature monitoring of the GIS contacts. In contrast, on-line monitoring technology has advantages in achieving real-time measurement of the contacts temperature so as to further carry out intelligent assessment of the load capacity and implement effective mitigation to the potential failure due to overheating. Infrared sensing method can realize non-intrusive temperature measurement without disturbance and destruction of the temperature field and thermal balance, and high-voltage and thermal isolation are also easy to be solved [12-13]. However, due to many reasons such as infrared absorption of the SF_6 gas, low thermal emissivity of polished metal conductor, environment of encapsulated high voltage, little research is done so far on infrared on-line temperature monitoring of GIS contacts. In addition, for the contacts being connected with an outer shield structure, the infrared method cannot directly sense the contacts temperature, which poses specific difficulty to the on-line monitoring applications.

To overcome the obstacles mentioned above regarding

† Corresponding Author: State Key Lab of Alternate Electrical Power System with Renewable Energy Sources, North China Electric Power University, Beijing, China. (lqmeee@ncepu.edu.cn)
* School of Electrical Engineering, Shandong University, Jinan, China. (conghaoxi@163.com)
** State Key Lab of Alternate Electrical Power System with Renewable Energy Sources, North China Electric Power University, Beijing, China. (taiwan1895.love@163.com, lbicb@163.com, lcr@ncpeu.edu.cn)
Received: December 6, 2013; Accepted: March 3, 2014

temperature measurement for GIS contacts, an on-line temperature monitoring method based on infrared sensing is proposed, and a real test platform is established to account for the influential factors as to improve the precision of infrared measurement. An artificial neural network algorithm is also adopted to deal with the quantitative temperature mapping among the contacts, the metallic shield and the environment. Finally, an integrated temperature monitoring system of the GIS contacts is developed and applied to on-site applications.

2. Technical Requirement in Infrared Temperature Measurement within GIS

The infrared sensing technology is a noninvasive instrumentation method, which is used to measure the temperature of an object by receiving the infrared radiation energy from the object. Basically, all objects above the absolute zero temperature are constantly radiating infrared energy into the surrounding space. The amount of the radiation energy and the distribution of the wavelength present a very close relationship with the surface temperature of the measured object. The higher the temperature of the object is, the greater the infrared radiation energy will be. If a small change happens in the temperature, there will be a significant change of the radiation energy. Hence, the surface temperature can be accurately determined by measuring the amount of the infrared radiation energy of the object.

However, some principal influential factors associated with the infrared sensing must be fully elucidated as to promote the field application of the above monitoring technology.

(1) Surface emissivity of the metal conductors. Most of the internal conductors within the GIS equipment are polished so as to improve the insulation level and avoid creeping discharge and partial discharge, however, the emissivity of the polished metals is quite low, such as aluminum or copper. Temperature measurement of the metal conductors requires an increased emissivity at the measured points.

(2) Absorption band of the SF_6 gas. In the GIS equipment, the infrared light radiated from the inner conductor can reach the infrared sensor only when it goes through the SF_6 gas absorption band. However, the SF_6 gas filled in the GIS equipment is a greenhouse gas with strong absorption effect to the infrared light. In order to improve the measurement accuracy and sensitivity, the absorption effect of the SF_6 gas should be minimized as much as possible.

(3) Difficulty in direct measurement of the contacts temperature. The GIS contacts are normally surrounded by a shield structure, hence, the infrared sensor can not sense the contacts directly.

Fig. 1. The established GIS test platform

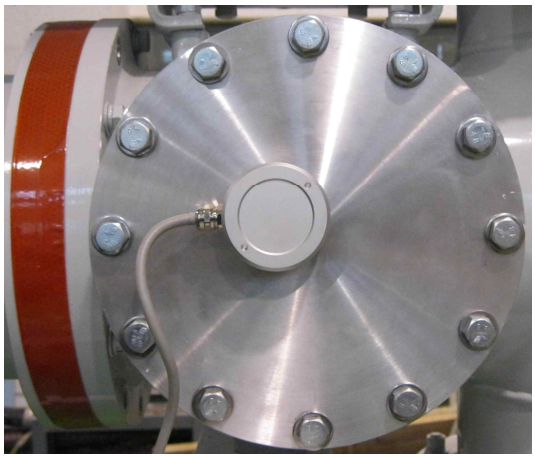

Fig. 2. Installation of the infrared sensor

In order to solve the above mentioned difficulties in the infrared measurement as well as facilitate experimental study on the influential factors, a GIS module-based test platform for on-line temperature monitoring of the contacts is established, as shown in Fig. 1. The GIS test platform includes a large current generator, an inside disconnecting switch, infrared sensors, etc. After a thorough survey, the HE-155A model infrared sensor, the emissivity of which is adjustable, is chosen as the sensing element for further experimental studies, as shown in Fig. 2. The infrared sensor is mounted on a metal cover at the inspection hole.

3. Influence of Metal Surface Emissivity on Infr ared Temperature Measurement

The surface emissivity of the polished metal is low, resulting in insufficient sensitivity in the on-line temperature measurement. An embedded scheme was proposed that, a round hole was cut out in the groove contact base and some substance with high stable chemical properties and high emissivity under SF_6 environment was embedded into the groove bottom [14]. Though this embedded scheme can avoid the limitations of aluminum

Fig. 3. Surface coating with infrared radiation paint

metal conductors and the infrared sensing can be converted to the measurement of ordinary materials, it will bring specific difficulties in the assembly process of the GIS equipment. Also, due to heat transfer process between the two materials, the embedded substance may not be able to reflect the contacts temperature change timely.

A surface coating method regarding the metal contacts is proposed in this paper to improve the infrared sensitivity. Normally, the radiation of metal conductors and other non-transparent material occurs within a few microns in the surface, and the emission rate is a function of the surface state, being independent of the surface size. Therefore, the surface emissivity of the radiation is determined by the coating substance itself other than the metal surface. In addition, the inner contacts temperature within GIS equipment is usually about 100℃ during normal operation, the emissivity of the radiation coating can be seen as approximately constant since the temperature range is not large. Here the HS-2-1 low-temperature non-metallic infrared radiation coating, as shown in Fig. 3, is adopted to improve the infrared radiation sensitivity. The surface coating is closely adhered to the metal conductor as to easily reach thermal equilibrium. Also, this method will not cause any problem of surface discharge or partial discharge. The radiation coating is made of carborundum, zircon ceramic powder and other special additives in the mixture. The coating is one kind of inorganic material with high melting point above 400 degrees Celsius and is hard to melt. The radiation coating can achieve excellent performance with a full-emissivity of 0.86. The coating thickness used in practice is less than 0.1mm, therefore, during normal condition of the GIS, the coating material and the conductor are in thermal equilibrium with exactly the same temperature, and the experiments have also proved this point.

4. Influence of SF_6 Gas Absorption on Infrared Temperature Measurement

As a greenhouse gas, the SF_6 gas has a strong absorption

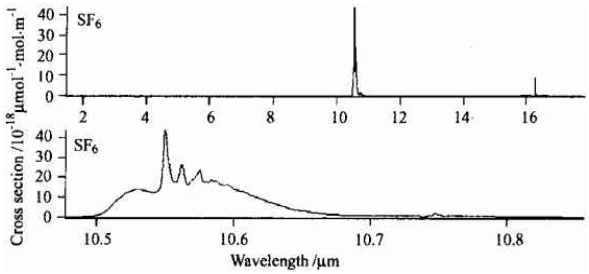

Fig. 4. Absorption spectrum of the SF_6 gas[11]

of the infrared radiation. As the infrared light radiated from the inner conductors passes through the SF_6 medium to reach the infrared sensor mounted at the inspection hole, an appropriate infrared band for measurement must be considerately selected to minimize the infrared absorption of SF_6 gas. As can be seen from Fig. 4, the SF_6 gas shows the strongest absorption effect around the center wavelength of 10.55μm [15]. Hence, the infrared sensor should be properly selected to avoid this absorption band. However, for practical applications, the experiments indicate that the absorption effect of SF_6 gas can be compensated by adaptively adjusting the emissivity of the infrared sensor as to guarantee the sensor readings consistently in good accordance with the actual temperature.

4.1 Influence of the SF_6 concentration on emissivity

The large current generator is used to provide an unchanged current flowing through the GIS contacts to maintain the temperature of the contacts (T=49.0℃), and then the SF_6 gas concentration is varied to observe the readings of the infrared sensor. Thereafter the emissivity of the infrared sensor is adjusted to make the reading consistent with the standard value, also verified by the thermocouples. The experimental results are shown in Table 1. For the GIS without SF_6 gas filling, the emissivity of the infrared sensor is set to 0.86, corresponding to temperature of 49℃, which is initially consistent with the infrared radiation coating.

As can be seen from Table 1, with increase of the SF_6 gas concentration, the infrared sensor reading reduces accordingly, which is due to increased absorption of the infrared light by the SF_6 gas. Hence, the emissivity of the infrared sensor should be adjusted as a compensation to maintain the accuracy of temperature measurement. At the scene, for a given specific SF_6 gas concentration, Table 1 can be used as a guidance to determine the infrared sensor emissivity by data fitting.

Table 1. Emissivity vs. Different SF_6 concentration (T= 49.0℃)

Concentration of SF_6 gas (MPa)	0	0.1	0.2	0.3	0.4
Sensor readings (℃)	49.0	37.5	24.3	12.0	6.0
Adapted emissivity	0.86	0.59	0.42	0.25	0.15

4.2 Influence of the infrared filter on sensor emissivity

In some cases the GIS is used to break large current, such as fault current, then high-temperature arc discharge will emerge between the contacts in the chamber. To counteract this, an infrared filter is installed at the fore-end of the infrared sensor to protect the probe from arc flow. In addition, the infrared filter can also filter out the interference band. However, the installation of the infrared filter needs to be checked to maintain the output accuracy of the infrared sensor. Experiments are carried out under a constant contacts temperature ($T = 36.2$℃) but with different concentration of the SF_6 gas. The infrared sensor emissivity is required to be adjusted until the sensor reading is consistent with the standard temperature value, as shown in Table 2.

Further, the output current of the large current generator is altered to change the contacts temperature, and then the SF_6 gas concentration is varied to observe the readings of the infrared sensor. The infrared sensor emissivity is also adjusted until the sensor reading is consistent with the actual temperatures, as shown in Table 3.

As can be seen from Table 3, with installation of the infrared filter, the emissivity of the infrared temperature sensor remains essentially unchanged when the contacts temperature is altered. This is mainly due to the nature of the infrared radiation coating itself, unlike the metal contacts material, the emissivity of which remains constant at different temperatures. Also, the infrared light absorption and radiation characteristics of the SF_6 gas remains unchanged as well at a certain concentration. In summary, the infrared absorbing effect of the SF_6 gas can be compensated by properly adjusting the emissivity of the infrared sensor, and the installation of the infrared filter will not affect the accuracy of the measured results, which promotes the further extensive application of the on-line infrared monitoring.

Table 2. Emissivity vs. SF_6 concentration with infrared filter (T=36.2℃)

Concentration of SF_6 gas (MPa)	0	0.1	0.2	0.3	0.4
Sensor readings (℃)	36.2	32.0	30.1	29.0	28.1
Adapted emissivity	0.86	0.65	0.62	0.58	0.55

Table 3. Emissivity vs. Different contact temperature with infrared filter

Concentration of SF_6 gas (MPa)	0	0.1	0.2	0.3	0.4
Adapted emissivity (T=36.2℃)	0.86	0.65	0.62	0.58	0.55
Adapted emissivity (T=44.0℃)	0.86	0.66	0.62	0.57	0.56
Adapted emissivity (T=61.0℃)	0.86	0.66	0.62	0.57	0.55

5. Temperature Mapping Between the Contacts and the Shield

The circuit breakers and disconnecting switches within the GIS module are normally equipped with a shield structure, which blocks the infrared sensor from sensing the contacts temperature directly. In that case, the following methodology is proposed in the paper. Firstly, based on establishment of the heat transfer model as well as experimental studies, the quantitative relationship between the temperature of the contacts and the metal shield can be achieved by data mapping. Then, direct infrared measurement can be done on the metal shield surrounding the contacts. Finally, the contacts temperature is thus obtained indirectly according to quantitatively data mapping. As shown in Fig. 5(a), the shield temperature (T1) can be directly obtained by the infrared sensor, and then the contacts temperature (T2) can be determined indirectly by the established mapping relationship. Fig. 5(b) shows the contacts and shield diagram in the disconnecting switch of the GIS test platform.

5.1 Establishment of the heat transfer model for GIS contact

For the disconnecting switch within the GIS module, the main structure parameters are given in Table 4 and the

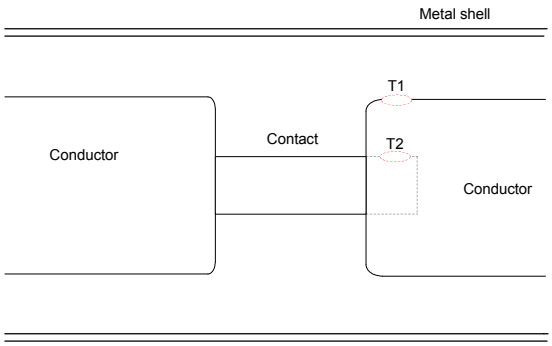

Fig. 5(a). Scheme for temperature measurement

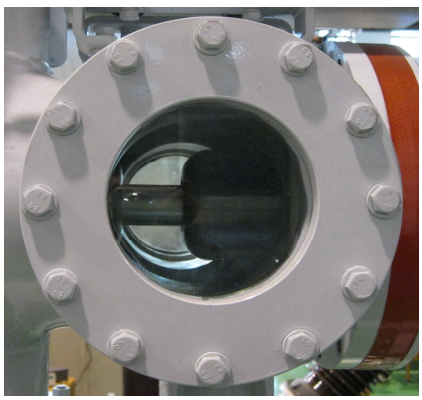

Fig. 5(b). Inner structure of the disconnecting switch

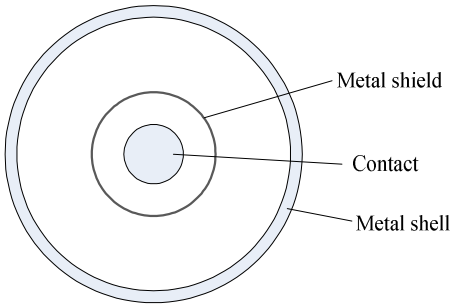

Fig. 6. Cross section of the disconnecting switch

Table 4. Basic parameters of the single-phase GIS disconnecting switch

Parameters	Values	Parameters	Values
Outer diameter of shell	260mm	Inner diameter of shield	105mm
Inner diameter of shell	248mm	Outer diameter of shield	109mm
Outer diameter of contact	43mm	Rated current	2000A

sectional diagram is shown in Fig. 6. The confined space between the internal contacts and the metal shell is filled with SF_6 gas.

The heat around the contacts is mainly generated by the current flowing through the contacts. The thermal dissipations include gas convection between the contacts and shield, heat conduction along the shield, gas convection between the shield and the shell, heat conduction along the shell, gas convection between the shell and the outside air. Here some assumptions are made to facilitate the modeling: 1) the metal contacts give off heat dissipation evenly, 2) the ambient temperature of the air far away from the GIS equipment is constant, and 3) the physical characteristic of the internal SF_6 gas remains unchanged.

For a two-dimensional modeling of the temperature field with natural gas convection, the temperature and velocity distribution are jointly governed by the general laws of mass transfer, momentum transfer and energy transfer, as is described by the following equations.

(1) Gas convection between the contacts and shield

The mass conservation equation:

$$\frac{\partial u_1}{\partial x}+\frac{\partial v_1}{\partial y}=0 \tag{1}$$

The momentum conservation equation:

$$\rho\left(\frac{\partial u_1}{\partial \tau}+u_1\frac{\partial u_1}{\partial x}+v_1\frac{\partial u_1}{\partial y}\right)=F_{x_1}-\frac{\partial p_1}{\partial x}+\eta\left(\frac{\partial^2 u_1}{\partial x^2}+\frac{\partial^2 u_1}{\partial y^2}\right) \tag{2}$$

$$\rho\left(\frac{\partial v_1}{\partial \tau}+u_1\frac{\partial v_1}{\partial x}+v_1\frac{\partial v_1}{\partial y}\right)=F_{y_1}-\frac{\partial p_1}{\partial y}+\eta\left(\frac{\partial^2 v_1}{\partial x^2}+\frac{\partial^2 v_1}{\partial y^2}\right) \tag{3}$$

The energy conservation equation:

$$\frac{\partial t_1}{\partial \tau}+u_1\frac{\partial t_1}{\partial x}+v_1\frac{\partial t_1}{\partial y}=\frac{\lambda}{\rho c_p}\left(\frac{\partial^2 t_1}{\partial x^2}+\frac{\partial^2 t_1}{\partial y^2}\right) \tag{4}$$

(2) Heat conduction along the shield

The differential heat conduction equation:

$$\frac{\partial^2 t_s}{\partial x^2}+\frac{\partial^2 t_s}{\partial y^2}=0 \tag{5}$$

(3) Gas convection between the shield and the shell

The mass conservation equation:

$$\frac{\partial u_2}{\partial x}+\frac{\partial v_2}{\partial y}=0 \tag{6}$$

The momentum conservation equation:

$$\rho\left(\frac{\partial u_2}{\partial \tau}+u_2\frac{\partial u_2}{\partial x}+v_2\frac{\partial u_2}{\partial y}\right)=F_{x_2}-\frac{\partial p_2}{\partial x}+\eta\left(\frac{\partial^2 u_2}{\partial x^2}+\frac{\partial^2 u_2}{\partial y^2}\right) \tag{7}$$

$$\rho\left(\frac{\partial v_2}{\partial \tau}+u_2\frac{\partial v_2}{\partial x}+v_2\frac{\partial v_2}{\partial y}\right)=F_{y_2}-\frac{\partial p_2}{\partial y}+\eta\left(\frac{\partial^2 v_2}{\partial x^2}+\frac{\partial^2 v_2}{\partial y^2}\right) \tag{8}$$

The energy conservation equation:

$$\frac{\partial t_2}{\partial \tau}+u_2\frac{\partial t_2}{\partial x}+v_2\frac{\partial t_2}{\partial y}=\frac{\lambda}{\rho c_p}\left(\frac{\partial^2 t_2}{\partial x^2}+\frac{\partial^2 t_2}{\partial y^2}\right) \tag{9}$$

(4) Heat conduction along the shield

The differential heat conduction equation:

$$\frac{\partial^2 t_w}{\partial x^2}+\frac{\partial^2 t_w}{\partial y^2}=0 \tag{10}$$

(5) Gas convection between the shell and the ambient air

The mass conservation equation:

$$\frac{\partial u_3}{\partial x}+\frac{\partial v_3}{\partial y}=0 \tag{11}$$

The momentum conservation equation:

$$\rho\left(\frac{\partial u_3}{\partial \tau}+u_3\frac{\partial u_3}{\partial x}+v_3\frac{\partial u_3}{\partial y}\right)=F_{x_3}-\frac{\partial p_3}{\partial x}+\eta\left(\frac{\partial^2 u_3}{\partial x^2}+\frac{\partial^2 u_3}{\partial y^2}\right) \tag{12}$$

$$\rho\left(\frac{\partial v_3}{\partial \tau}+u_3\frac{\partial v_3}{\partial x}+v_3\frac{\partial v_3}{\partial y}\right)=F_{y_3}-\frac{\partial p_3}{\partial y}+\eta\left(\frac{\partial^2 v_3}{\partial x^2}+\frac{\partial^2 v_3}{\partial y^2}\right) \tag{13}$$

The energy conservation equation:

$$\frac{\partial t_3}{\partial \tau}+u_3\frac{\partial t_3}{\partial x}+v_3\frac{\partial t_3}{\partial y}=\frac{\lambda}{\rho c_p}\left(\frac{\partial^2 t_3}{\partial x^2}+\frac{\partial^2 t_3}{\partial y^2}\right) \tag{14}$$

For the parameters with different subscripts in the above formula, u and v denote the velocity components along x and y directions, ρ is the density of the gas, c_p is the specific heat of the gas, λ is the thermal conductivity of the gas, p is the gas pressure, F_x and F_y are the volume force components along x and y directions, η is the kinematic viscosity coefficient of the gas, t denotes the temperature.

The boundary conditions for the modeling are set as:

$$t(x,y)|_{x^2+y^2=\infty}=t_\infty,\quad u(x,y)|_{x^2+y^2=\infty}=0,$$
$$v(x,y)|_{x^2+y^2=\infty}=0,\quad p(x,y)|_{x^2+y^2=\infty}=0,$$
$$t(x,y)|_{x^2+y^2=r_{so}^2}=t_{so},\quad u(x,y)|_{x^2+y^2=r_{so}^2}=0,$$
$$v(x,y)|_{x^2+y^2=r_{so}^2}=0,\quad p(x,y)|_{x^2+y^2=r_{so}^2}=0,$$

t_∞ denotes the ambient temperature, and t_{so} represents the shield temperature of the outer surface.

The thermal analysis can be used to analyze the factors which may affect the quantitative temperature relationship among the shields, the contacts and the ambient environment, so as to determine the physical quantities to be monitored in the experimental studies. With the imposed boundary conditions, the above differential equations can be solved with the ANSYS software as to simulate the temperature distribution of the contacts and the shield. A radial display of the temperature distribution from inside to outside, namely the switch contacts, the shield and shell, is shown in Fig. 7. The temperature distribution and the difference between the contacts and the shields can be clearly recognized, and this model is used to preliminarily study and determine the temperature relationship between the contacts and the shield. The thermal analysis and ANSYS simulation can also present guidance in implementing the proposed method as to indirectly obtain the contacts temperature by directly sensing the metal shield surrounding the contacts.

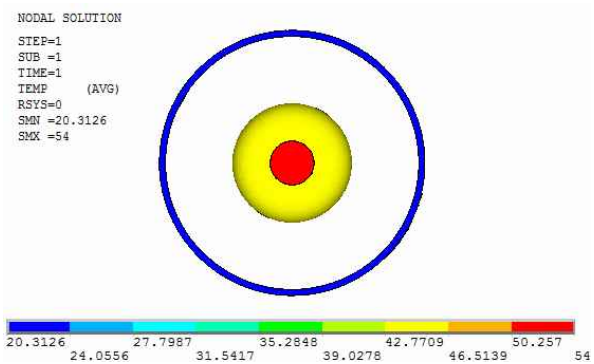

Fig. 7. Radial diagram of the temperature distribution within the GIS equipment

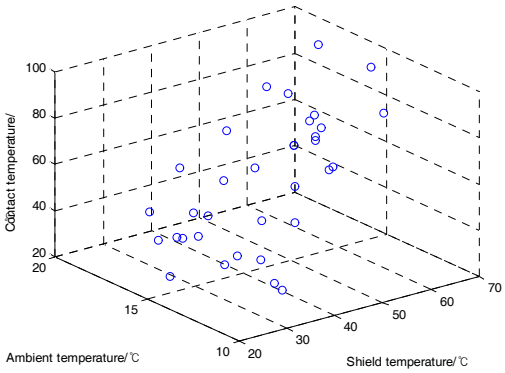

Fig. 8. Temperature mapping between the contact and the shield

5.2 Experimental study

As shown in Fig. 5(a), two calibrated thermocouples are implanted on the shield (T1) and the contacts (T2) inside the GIS, and the output of the large current generator is adjusted to alter the contacts temperature, then the sensors' stable readings are retained. The experiments are also carried out under different ambient temperature to see the nonlinearities. With enough experimental data, the temperature mapping curve of the contact and the shield can be obtained. As an example, Fig. 8 gives a schematic show of the 3-D temperature mapping, including the contacts, the shield and the ambient temperature. Theoretically, the nonlinear behavior is mainly due to the change of the ambient temperature.

5.3 Temperature mapping based on ANN algorithm

The artificial neural network (ANN) algorithm has been widely applied in a large number of engineering practices [16-17], which presents high degree of self-learning, self-organizing and adaptive capacities. Without having to know the precise model, the ANN can approximate the multidimensional nonlinear relationship between the input and the output vectors. Actually for the GIS study, due to the varying factors including current flow, ambient temperature and so on, nonlinear behavior may arise, where the ANN method will be a good choice. Here, the BP neural network structure is adopted in this paper to establish the mapping relationship between the contacts and the shield temperature, as is shown in Fig. 9.

30 sets of data obtained by the experiment are used as the ANN training samples, and the other 5 sets are randomly chosen for the testing purpose. In the designed BP ANN, the input vectors include the shield temperature and the ambient temperature, while the output vector is the contacts temperature. There are two hidden layers used in the present study, where the first hidden layer neurons is twelve and the second hidden layer neurons is one. The hidden layer neurons are defined by the following formula $L=\sqrt{n_i+n_o}+e$, in which L is the hidden layer

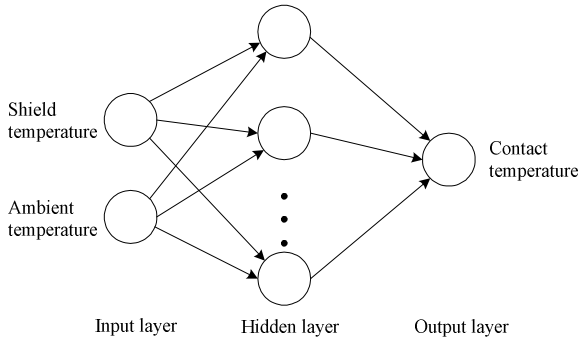

Fig. 9. BP ANN model for the temperature mapping

Table 5. Comparison between test samples and neural network prediction

(Shield temperature, ambient temperature)	Predicted results	Measured values	Relative errors
(35.3, 15.7)	44.2	45.1	2.0%
(35.1, 16.4)	43.7	43.7	0
(69.1, 18.5)	90.6	89.9	0.8%
(69.0, 15.6)	91.6	90.6	1.1%
(53.6, 16.4)	70.4	71.2	1.1%

neurons, n_i is the input layer neruons, n_o is the output layer neruons, and e can be any constant ranging from 1 to 10. In the present study, the parameters of n_i, n_o and e are respectively set as 3, 1 and 10. The alternating gradient BP learning process based on the Levenberg-Marquardt algorithm is used as the convergence criterion to train the weight coefficient and the threshold of the BP ANN. The learning rate is set to 0.1. After 50 training iterations, the training error converges quickly to a small value, indicating that the training algorithm is fast and effective.

Hence, the 5 additional sets of data are taken to verify the trained BP network, and the predicted results are given in Table 5, which indicate the contacts temperature can be accurately predicted by the BP network according to the shield and the ambient temperature. Despite slight difference between the predicted results and actual data, within the range of an allowable error below 2%, the prediction accuracy is excellent and sufficient for practical applications.

6. Implementation of the On-line Infrared Monitoring System for GIS Contacts

Based on the above proposed technologies, the authors have developed an on-line infrared temperature monitoring device for the GIS contacts, as is schematically shown in Fig. 10, which consists of a metal shell, a sealed cover, an infrared sensor and an infrared glass filter installed at the front of the sensor probe. The infrared radiation coating is coated on the switch contacts to improve the emissivity of the measured objects. Here, the temperature of the shield is directly sensed and the contacts temperature is determined

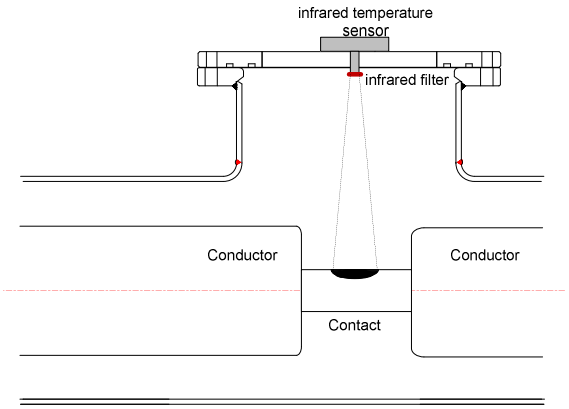

Fig. 10. Schematic diagram of the on-line infrared sensing device

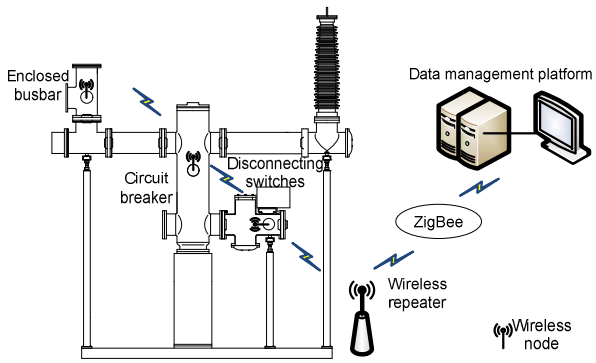

Fig. 11. Design of the on-line infrared monitoring system for GIS contacts

indirectly by means of ANN mapping. The infrared filter is installed at the fore-end of the infrared sensor, with a view to filtering out the interference band and avoiding possible impact from high-temperature arc flow. The metal shell is designed with a circular shape, projecting outwardly to ensure a safe distance between the metal conductor and the probe. The junction between the sealing cover and the metal shell is composed of a rubber ring, the sealants and screws to achieve a good sealing system.

The integrated on-line monitoring system is shown in Fig. 11. The infrared sensor is equipped with wireless transmitter module, and the ZigBee network is selected as the wireless communication path with unique advantages in anti-interference, long communication distance and short delay. The design of the on-line monitoring system is divided into hardware system and software system. The hardware comprises infrared sensor, data acquisition and transmission module, signal relay point and data management platform. The software includes temperature data acquisition program, wireless communication program and data management program. The temperature acquisition and transmission system mainly includes temperature acquisition device and wireless data transmission devices. The type of the infrared sensor used in the temperature acquisition device is HE-155A. The measurement range is 0～500℃, the accuracy is ±1℃ and the response time is

500ms. The CC2430 SoC chip made by Chipcon corporation is used as the signal relay point, which is powered by a built-in battery. Finally, the real-time temperature data is received by the wireless data receiver, and then it is transmitted to the data management system. The wireless data receiver can support RS232/RS485 bus communication mode and a dynamically adjustable frequency. The data management system presents features of online-collection, over-temperature analysis, temperature trend analysis and temperature gradient analysis. The collected infrared data is firstly transmitted through the wireless transmitters, and then it is relayed by the wireless repeater to the data management system. As a result, the temperature change of the contacts can be observed at the console side instantaneously, achieving continuous and automatic measurement of the GIS contacts temperature as for timely warning or prognosis to be made.

This on-line temperature monitoring system has been put into application in a few HV substations operational in North and Middle China, which demonstrates effectiveness of the proposed technology. Further, the monitored temperature data of the GIS contacts will form a basis for intelligent load assessment and smart load shedding, with a view to exploring and making full use of the loading capacity of the power system with regard to different operational conditions.

7. Conclusion

Long-term overheating of the GIS contacts may lead to major accidents, posing severe threat to the electrical equipment and the power system. An on-line temperature monitoring system based on infrared sensing has been developed in this paper for on-site applications.

(1) For the special structure of GIS, an infrared sensing scheme is proposed, and a test platform for on-line temperature monitoring of the GIS contacts is set up. Experimental studies are carried out to elucidate and justify the impacts of several influential factors so as to guarantee the infrared sensitivity and accuracy.

(2) For the GIS contacts surrounded with a shield structure, a methodology is proposed by directly measuring the shield temperature and indirectly determine the contacts temperature based on ANN mapping. The ANN algorithm is introduced to establish the quantitative relationship between the contacts, the shield and the ambient temperature.

(3) An integrated on-line infrared temperature monitoring system has finally implemented, which recurs to the ZigBee network to realize wireless communication of the monitored temperature data to the console side for further processing. From the temperature point of view, the designed system also lays a basis for intelligent load assessment and smart load shedding with regard to complex conditions.

Acknowledgements

Financial support by the National High Technology Research and Development Program of China (2011 AA05A121), the Natural Science Foundation of China (51277061) is here all acknowledged.

References

[1] Fang Shuhua, Lin Heyun, Ho S.L., Wang Xianbing, Jin Ping, Huang Yunkai, Yang Shiyou, "Contact parameter computation and analysis of air circuit breaker with permanent magnet actuator," *Journal of Electrical Engineering and Technology*, vol. 8, no. 3, pp. 595-602, 2013.

[2] Seo Hun-Chul, Jang Won-Hyeok, Kim Chul-Hwan, Chung Young-Hwan, Lee Dong-Su, Rhee Sang-Bong, "Analysis of magnitude and rate-of-rise of VFTO in 550 kV GIS using EMTP-RV," *Journal of Electrical Engineering and Technology*, vol. 8, no. 1, pp. 11-19, 2013.

[3] Kim Joong-Kyoung, Oh Yeon-Ho, Lee Ji-Yeon, Hahn Sung-Chin, "Temperature rise prediction of GIS bus bar considering thermal flow," *Transactions of the Korean Institute of Electrical Engineers*, vol. 58, no. 4, pp. 742-747, 2009.

[4] Wu Xiaowen, Li Hongtao, Peng Yunfeng, Xie Zhiyang, Jin Xiangchao, "Temperature distribution analysis of single-phase GIS bus," in *Asia-Pacific Power and Energy Engineering Conference*, pp. 1-4, 2011.

[5] Ogawa Takuya, Murakawa Saburo, Nishina Daisaku, Tanaka Takahiro, Fukagawa Kenta, Takahashi Ichiro, "A study on the effect of land use and insolation environment on surrounding air temperature in mountain area: Measurement results and analysis by GIS," *AIJ Journal of Technology and Design*, vol. 17, no. 35, pp. 245-248, 2011

[6] H. K. Kim, Y. H. Oh, and S. H. Lee, "Prediction of Temperature Rise in Gas Insulated Busbar Using Multi-Physics Analysis," in *Transmission and Distribution Conference and Exposition-Asia and Pacific*, pp. 1-4, Oct. 2009.

[7] C. T. Dervos, P. Vassiliou, and J. A. Mergos, "Thermal stability of SF_6 associated with metallic conductors incorporated in gas insulated switchgear power substations," *Journal of Physics D-Applied Physics*, vol. 40, no. 2, pp. 6942-6952, 2007.

[8] E. H. Choi, K. C. Kim, and K. S. Lee, "Breakdown Characteristics of SF_6 and Liquefied SF_6 at Decreased Temperature," *Journal of Electrical Engineering & Technology*, vol. 7, no. 5, pp. 765-771, Sep. 2012.

[9] S. Heng, Z. Liu, X. Li, and J. Wang, "Investigation on breakdown characteristics in contact gap for vacuum interrupters on area effect," *High Voltage Apparatus*, vol. 43, no. 3, pp. 161-164, 2007.

[10] X. Shi, W. Zha, F. Sun, X. Wang, and Q. Zhang,

"Inner temperature distribution of UHV GIS using infrared thermo-diagnosis technology," *High Voltage Engineering*, vol. 33, no. 6, pp. 16-20, 2007.

[11] H. Chen and S. Hou, "Infrared diagnostics of power equipment failure," *China Electric Power Press*, Beijing, 1999.

[12] T. Barry, G. Fuller, K. Hayatleh, and J. Lidgey, "Self-Calibrating Infrared Thermometer for Low-Temperature Measurement," *IEEE Transactions on Instrumentation and Measurement*, vol. 60, pp. 2047-2052, 2011.

[13] R. Kurte, C. Beyer, H. M. Heise, and D. Klockow, "Application of infrared spectroscopy to monitoring gas insulated high-voltage equipment: Electrode material-dependent SF_6 decomposition," *Analytical and Bioanalytical Chemistry*, vol. 373, pp. 639-646, 2002.

[14] S. Wu, Y. Zheng, Z. Chen, "An on-line monitoring scheme of conductor temperature in GIS based on infrared temperature measurement," *High Voltage Apparatus*, vol. 45, no. 4, pp. 100-102, 2009.

[15] D. Wang, Q. Wei, S. Liu, W. Fang, and W. Feng, "Method of detecting concentration of SF_6 in GIS by absorption of infrared laser," *Journal of Atmospheric and Environmental Optics*, vol. 3, no. 2, pp. 139-141, 2008.

[16] Moon Jin Woo, Lee Ji-Hyun, Yoon Younju, Kim Sooyoung, "Determining optimum control of double skin envelope for indoor thermal environment based on artificial neural network," *Energy and Buildings*, vol. 69, pp. 175-183, 2014.

[17] I. Ozturk Hande, M. Emin Kutay, "An artificial neural network model for virtual Superpave asphalt mixture design," *International Journal of Pavement Engineering*, vol. 15, no. 2, pp. 151-162, 2014.

Qingmin Li is now a professor in electrical engineering at North China Electric Power University, China. He graduated from Tsinghua University, China, where he got his degrees of BSc (1991), MSc (1994) and PhD (1999) in electrical engineering. He joined Tsinghua University as a lecturer in 1996, and came to the UK in 2000 as a postdoctoral research fellow working at Liverpool University and later at Strathclyde University. He joined Shandong University in 2003 and worked there as a professor in electrical engineering till 2011. He also worked at Arizona State University, USA, as a visiting professor from February to August 2010. His special fields of interest include high-voltage engineering, applied electromagnetics, condition monitoring and fault diagnostics, high-voltage power electronics, etc. He is a member of IET and IEEE.

Haoxi Cong graduated in 2011 with a first honor degree of BSc in electrical engineering from Shandong University, China. He is now studying there for his PhD degree, with a specific research interest in secondary arc within half-wave length transmission lines and the interaction mechanism with the electromagnetic transients of power system.

Xing Jinyuan received the B.Sc. degree in electrical engineering from Jilin University, Changchun City, China, in 2012 and is currently pursuing the M.Sc. degree in electrical engineering from North China Electric Power University, Beijing, China, with a specific research interest in secondary arcs with half-wavelength transmission lines.

Bo Qi was born in Shandong Province, China, on November 28, 1980. He received the B.S. degree in electric al engineering, the M.S. degree in high voltage and insulation, and the Ph.D. degree in high voltage and insulation from North China Electric Power University, Beijing, China, in 2003, 2006, and 2010, respectively. Currently, he is a Lecturer in the School of Electric and Electronic Engineering, North China Electric Power University. His current research interest is in condition monitoring of power apparatus.

Chengrong Li (SM'03) was born in Xian, China, on March 1, 1957. He received the B.S. and M.S. degrees in electrical engineering from North China Electric Power University (NCEPU), Beijing, China, in 1982 and 1984, respectively, and the Ph.D. degree in elec-trical engineering from Tsinghua University, Beijing, in 1989. He joined the University of South Carolina, Beau-fort, in 1992 as a Postdoctoral Research Fellow. He joined NCEPU in 1995. Currently, he is a Professor in the Department of Electrical Engineering, NCEPU. His current research interests include gas discharge, electrical insulation and materials, and condition monitoring of power apparatus. Dr. Li is a Fellow of the Institute of Electrical Engineers.